



# Orphan GRB Afterglow Searches with the Pan-STARRS1 COSMOS Survey

Yun-Jing Huang<sup>1</sup>, Yuji Urata<sup>2</sup>, Kuiyun Huang<sup>3</sup>, Kuei-sheng Lee<sup>4</sup>, Meng-feng Tsai<sup>4</sup>, Yuji Shirasaki<sup>5,6</sup>, Marcin Sawicki<sup>7</sup>,  
Stephane Arnouts<sup>8</sup>, Thibaud Moutard<sup>7</sup>, Stephen Gwyn<sup>9</sup>, Wei-Hao Wang<sup>10</sup>, Sebastien Foucaud<sup>11</sup>, Keiichi Asada<sup>10</sup>,  
Mark E. Huber<sup>12</sup>, Richard Wainscoat<sup>12</sup>, and Kenneth C. Chambers<sup>12</sup>

<sup>1</sup> Department of Physics, National Taiwan University—No. 1, Sec.4 Roosevelt Road, Taipei 10617, Taiwan; [yunjinghuang14@gmail.com](mailto:yunjinghuang14@gmail.com)

<sup>2</sup> Institute of Astronomy, National Central University, Chung-Li 32054, Taiwan; [urata@g.ncu.edu.tw](mailto:urata@g.ncu.edu.tw)

<sup>3</sup> Center for General Education, Chung Yuan Christian University, Taoyuan 32023, Taiwan

<sup>4</sup> Department of Computer Science & Information Engineering, National Central University, Chung-Li 32054, Taiwan

<sup>5</sup> National Astronomical Observatory of Japan, 2-21-1 Osawa, Mitaka, Tokyo 181-8588, Japan

<sup>6</sup> Department of Astronomical Science, School of Physical Sciences, SOKENDAI (The Graduate University for Advanced Studies), 2-21-1 Osawa, Mitaka, Tokyo 181-8588, Japan

<sup>7</sup> Institute for Computational Astrophysics & Department of Astronomy and Physics, Saint Mary's University, Halifax, Canada

<sup>8</sup> Aix Marseille Université, CNRS, Laboratoire d'Astrophysique de Marseille, UMR 7326, F-13388, Marseille, France

<sup>9</sup> NRC-Herzberg, 5071 West Saanich Road, Victoria, British Columbia V9E 2E7, Canada

<sup>10</sup> Academia Sinica Institute of Astronomy and Astrophysics, Taipei 106, Taiwan

<sup>11</sup> Department of Astronomy, Shanghai Jiao Tong University, Dongchuan RD 800, 200240 Shanghai, People's Republic of China

<sup>12</sup> Institute for Astronomy, University of Hawaii at Manoa, Honolulu, HI 96822, USA

Received 2020 January 4; revised 2020 April 29; accepted 2020 April 30; published 2020 July 2

## Abstract

We present the result of a search for orphan gamma-ray burst (GRB) afterglows in the Pan-STARRS1 (PS1) COSMOS survey. There is extensive theoretical and observational evidence suggesting that GRBs are collimated jets; the direct observation of orphan GRB afterglows would further support this model. An optimal survey strategy is designed by coupling the PS1 survey with the Subaru/Hyper-Suprime-Cam (HSC) survey. The PS1 COSMOS survey, one of the survey fields in the PS1 Medium Deep Survey (PS1/MDS), searches a field of 7 deg<sup>2</sup> from 2011 December to 2014 January, reaching a limiting magnitude  $R \sim 23$ . The dense cadence of PS1/MDS is crucial for identifying transients, and the deep magnitude reached by the HSC survey ( $R \sim 26$ ) is important for evaluating potential GRB hosts. A transient classification method is employed to select potential orphan GRB afterglow candidates. After a thorough analysis of the transient and host galaxy properties, we conclude that there are no candidates in this survey field. The null result implies that the consideration of jet structures is essential for further orphan GRB afterglow surveys.

*Unified Astronomy Thesaurus concepts:* Gamma-ray bursts (629); Transient sources (1851); Time domain astronomy (2109)

## 1. Introduction

Gamma-ray bursts (GRBs) are highly energetic explosions involving compact objects; they are caused by mergers or by the core collapse of massive stars (e.g., Piran 1999). Jet collimation is needed to explain the large amount of isotropic equivalent energy released in the comparatively short prompt gamma-ray phase of GRBs (e.g., Sari et al. 1999; Frail et al. 2001). Furthermore, cocoon structures around ultrarelativistic jets are also identified (Izzo et al. 2019; Chen et al. 2020). Off-axis orphan afterglows (OAs) are a natural consequence of GRB jet production (Rhoads 1999), and the confirmed off-axis origin of X-ray flashes (XRFs) also indicates the existence of OAs (e.g., Granot et al. 2002, 2005; Yamazaki et al. 2002; Urata et al. 2015). For both populations of the GRBs, short and long GRBs, unification along with the GRB jet viewing angle is essential, similar to the active galactic nucleus (AGN) model (Antonucci 1993). Urata et al. (2015) verified XRFs as the off-axis viewing of long GRBs based on both the prompt emission (i.e., lower peak energy of prompt spectrum and energetic) and afterglow (i.e., multicolor brightening and supernova (SN) association) properties; thus, further verification of off-axis viewing of GRBs at the larger viewing angle (i.e., OAs) is crucial for unification of GRBs, including related stellar explosions. In particular, off-axis viewing of classical short GRBs is essential to reveal the nature of short GRBs associated with gravitational wave transients caused by compact star

mergers (Lamb et al. 2018; Lamb & Kobayashi 2017, 2019). It is notable that most theoretical models for GW170817/GRB 170817A employed the complicated jet structure with off-axis viewing (e.g., Alexander et al. 2017; Haggard et al. 2017; Lazzati et al. 2017; Murguia-Berthier et al. 2017; Ioka & Nakamura 2018; Jin et al. 2018; Kathirgamaraju et al. 2018; Troja et al. 2018, 2019; Lamb & Kobayashi 2018; Lyman et al. 2018; Lamb et al. 2019).

The mechanism of the collimated jet model is as follows: Relativistic matter with Lorentz factor  $\Gamma$  is ejected as a jet with opening half-angle  $\theta_{\text{jet}}$ . Radiation, on the other hand, is beamed into a cone with opening angle  $\Gamma^{-1}$ , which is initially inside the jet. Depending on the observation angle  $\theta_{\text{obs}}$ , the prompt emission will shift to the lower-frequency side or become invisible at  $\theta_{\text{obs}} > \theta_{\text{jet}}$ . As  $\Gamma$  decreases, the radiation cone spreads, giving rise to an afterglow emission, with wider angular range and fainter magnitude than the initial prompt emission. When  $\Gamma^{-1}$  exceeds  $\theta_{\text{jet}}$ , it will cause two observable effects, dependent on the observation angle  $\theta_{\text{obs}}$ : (1) achromatic breaks in the light curves for on-axis observers ( $\theta_{\text{obs}} < \theta_{\text{jet}}$ ); and (2) the appearance of off-axis OAs for off-axis observers ( $\theta_{\text{obs}} > \theta_{\text{jet}}$ ). Although chromatic temporal afterglow evolution from X-ray to optical is one of the puzzles of GRB physics, the observation of achromatic breaks in a number of GRB afterglows supports the existence of jet collimation (e.g., Harrison et al. 1999); the finding of OAs would provide additional direct observational evidence for it.

The event rate of OAs depends on the jet structure. Nakar et al. (2002, hereafter N02) considered GRBs to have constant total energy and a universal post-jet-break light curve, with jets having a constant maximal observing angle  $\theta_{\max}$  that is independent of  $\theta_{\text{jet}}$  in the case of  $\theta_{\text{jet}} < \theta_{\max}$ , and derived the maximal flux at  $\theta_{\text{obs}}$  to estimate the event rate at the limiting magnitude of observing instruments. Totani & Panaitescu (2002, hereafter T02) used average GRB parameters from a sample of 10 well-studied events, and estimated the event rate in the framework of the collimated jet model. Both of these studies considered a uniform jet with sharp edges: the “top-hat” model. Rossi et al. (2008, hereafter R08), on the other hand, considered a jet with a wide outflow angle  $\theta_{\text{jet}} = 90^\circ$  and an angle-dependent energy distribution  $E(\theta) \propto \theta^{-2}$ , the universal structured jet (USJ) model. The predicted rates from the three papers differ by about an order of magnitude for an all-sky snapshot at a given observational sensitivity in optical range (R08, Figure 8). Therefore, systematic surveys for off-axis OAs differentiate between the models by constraining the event rate.

Previous failed attempts at OA searches have been numerous in various wavelengths: X-ray (e.g., Grindlay 1999; Greiner et al. 2000), optical (e.g., Rau et al. 2006; Malacrino et al. 2007), and radio band (e.g., Levinson et al. 2002; Gal-Yam et al. 2006). Grindlay (1999) found 13 candidates in the Ariel 5 survey and set the all-sky event rate to  $\sim 0.15 \text{ day}^{-1}$ , which is consistent with BATSE. Greiner et al. (2000) found 23 candidates in the ROSAT all-sky survey, but these were later shown to be mostly, if not entirely, from flare stars. These results indicate that there is no marked difference between the beaming angles of prompt gamma-ray and X-ray emissions. There have been several optical surveys searching for OAs using different sky coverage and observation depths. The Deep Lens Survey transient search reached a sensitivity of 24 mag and surveyed an area of  $0.01 \text{ deg}^2 \text{ yr}$  (Becker et al. 2004). Rykoff et al. (2005) surveyed a wide field of effective coverage  $1.74 \text{ deg}^2 \text{ yr}$  (but with a low sensitivity of 17.5 mag) using the ROTSE-III telescope. Rau et al. (2006) used the Wide Field Imager (WFI) attached to the 2.2 m MPG/ESO telescope to survey an area of  $12 \text{ deg}^2$ , with a sensitivity as low as  $R = 23$  mag. They observed for 25 nights with a one- or two-night separation. Malacrino et al. (2007) performed a search using the CFHTLS very wide survey with a sensitivity as low as  $R = 22.5$  mag and an area of  $490 \text{ deg}^2$ . However, all these attempts have failed to provide a firm detection of off-axis OAs, null results are in agreement with theoretical predictions (e.g., T02). Recently, Law et al. (2018) reported the discovery of a radio transient that has properties similar to either a magnetic nebula or an OA, with the evidence strongly suggesting the latter; Marcote et al. (2019), by examining source properties, later supported the idea that this radio transient is likely an OA.

In this paper we report a systematic survey of OAs using Pan-STARRS1. The paper is structured as follows. In Section 2, we describe our observational strategy: coupling the Pan-STARRS1 and Subaru/Hyper-Suprime-Cam (HSC) surveys. In Section 3, we explain the details of the instrumentation and the survey duration. In Section 4, we describe our transient classification method and our analysis of photometric redshifts (zphot) using the Le Phare program (Arnouts et al. 1999; Ilbert et al. 2006) and present our results. In Section 5, we discuss the predicted detection rates from three theoretical papers and compare them with our result; we also

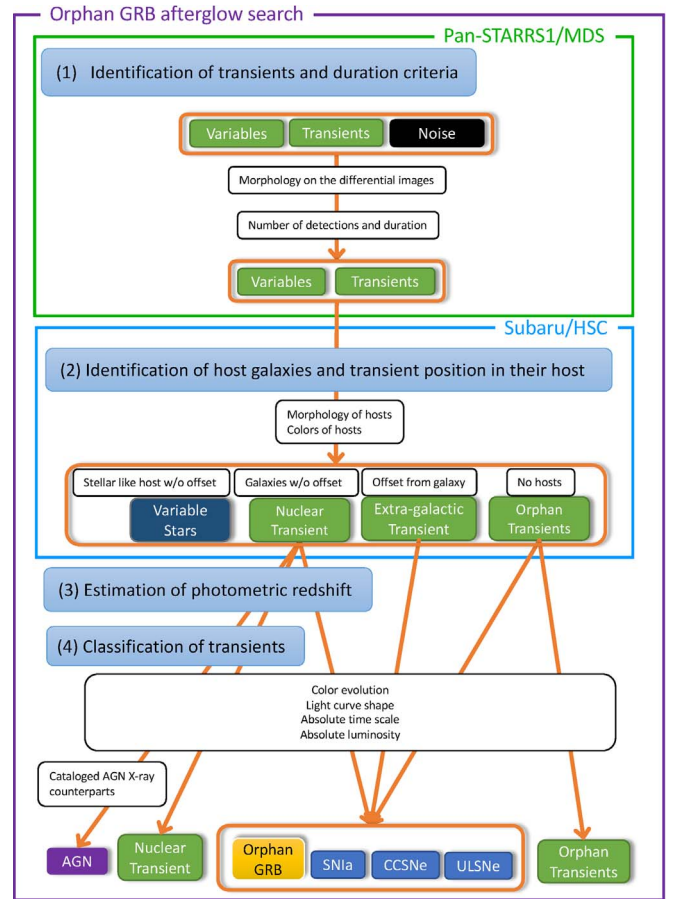


Figure 1. Strategy of survey.

calculate OA rates for future prospective surveys such as HSC and LSST. Finally, we present our conclusions in Section 6.

## 2. Survey Strategy

The expected properties of an OA are (1) the absence of prompt emissions in the high energy band; (2) a brightness fainter than that of on-axis GRB afterglows; (3) a light curve with three components (rise, peak, and rapid decay); (4) the same optical color as on-axis afterglows; and (5) an association with a host galaxy having properties similar to the host galaxies of on-axis GRBs. Taking these properties into account, we designed OA searches using Pan-STARRS1 and HSC. Our basic search procedure is shown in Figure 1. Similar to detections of prompt emission with the uniform spatial distributions of GRB on the celestial sphere, surveys using wide field of view (FOV) detectors with larger than several thousand square degrees such as Swift/BAT (1.4 steradian (half coded); Barthelmy et al. 2005) and *HETE-2*/WXM ( $80^\circ \times 80^\circ$ ; Shirasaki et al. 2003) are desired for efficient OA searches. However, because of the long lifetimes of the afterglows, the FOV of instruments can be reduced by using tiled observations with the appropriate cadence and pattern. Therefore, untargted transient surveys with optical wide-field imagers, such as the PanSTARRS1 Medium Deep Survey (MDS) and the Subaru/HSC, are sufficient for these searches.

One of the challenges for such generic optical transient surveys is distinguishing OAs from other types of optical transients, because candidates are expected to be rare compared with SNe of known types. We designed a seven-step procedure

for finding OAs: (1) creating differential images using reference-stacked and nightly stacked images, (2) generating light curves for transient components, (3) identifying host galaxies, (4) measuring transient locations in hosts, (5) matching with known sources in various catalogs, (6) matching of light and color temporal evolution patterns, and (7) estimating of the photometric redshifts of hosts. These selections have also been providing other rare transient phenomena (e.g., Urata et al. 2012; Tanaka et al. 2014; Cenko et al. 2015).

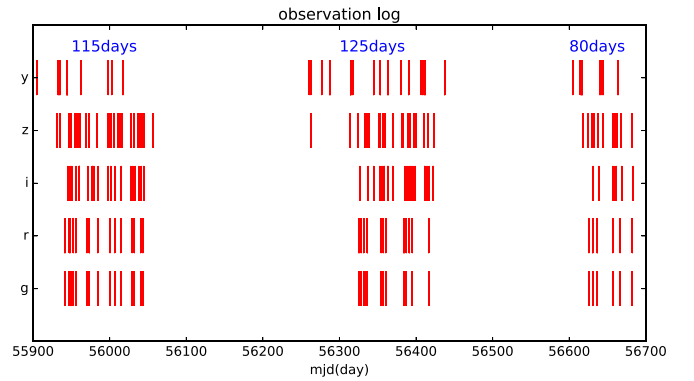
We used Pan-STARRS1/MDS for finding transients and characterizing their light curves and colors, and Subaru HSC for identifying host galaxies and obtaining photometric redshifts. The dense and continuous monitoring ability of the Pan-STARRS1/MDS fields is crucial, given the duration of the expected OAs. Considering the limiting magnitudes of Pan-STARRS1/MDS, the expected observable duration width is about one or two weeks, relatively short compared to the typical variable timescale of AGN and SN. The multicolor observing capability of Pan-STARRS1/MDS is crucial for characterizing light curves and colors. The colors of classical GRB afterglows (e.g.,  $g-r = 0.5 \pm 0.2$ ,  $r-i = 0.6 \pm 0.2$ ; Šimon et al. 2001; Li et al. 2018) exhibit no temporal evolution and no redshift dependency, because these emission mechanisms of optical afterglows, unlike that of other transients, is synchrotron radiation, usually describable by a simple power law. Given the limiting magnitude of Pan-STARRS1/MDS, the expected redshift range of OAs is  $z \sim 1$ . The brightness range of host galaxies for classical GRBs at  $z$  up to  $\sim 1$  is from 23.0 to 25.5 mag in  $r'/R$  band (e.g., Berger 2010), which Subaru/HSC images are deep enough to detect.

### 3. Observation and Data

#### 3.1. Pan-STARRS1 Survey

Pan-STARRS1 (PS1) is a 1.8 m telescope located at the summit of Haleakala on the island of Maui, Hawaii. It performs a wide field optical sky-survey with an FOV of 7 square degrees using a mosaic CCD camera with sixty  $4800 \times 4800$ -pixel detectors ( $0''.26$  per pixel). The full description of the system is given in Tonry et al. (2012) and Chambers et al. (2016). PS1 uses five broadband filters, designated as  $g_{P1}$ ,  $r_{P1}$ ,  $i_{P1}$ ,  $z_{P1}$ , and  $y_{P1}$ . The first four are similar to the SDSS filters  $g_{SDSS}$ ,  $r_{SDSS}$ ,  $i_{SDSS}$ , and  $z_{SDSS}$ , but different in that  $g_{P1}$  extends 20 nm redward of  $g_{SDSS}$  and  $z_{P1}$  is cut off at 920 nm. The range of  $y_{P1}$  is roughly from 920 nm to 1050 nm. Further information on the filter and photometric system is given in Tonry et al. (2012).

The PS1 Medium Deep Survey (MDS) surveyed 10 fields, each with an area of 7 square degrees. In this work we evaluate the MD04 field of PS1 MDS, which is centered at R.A. (J2000) =  $150^\circ 00'$ , decl.(J2000) =  $2^\circ 20'$ , and overlaps a well-studied field, the COSMOS field. We can make use of the extensive multiband data from other surveys to classify our transients. The cadence and filter cycle are as follows: Each night three to five MD fields are observed, using both  $g_{P1}$  and  $r_{P1}$  on the first night,  $i_{P1}$  on the following night, and  $z_{P1}$  on the third.  $y_{P1}$  is used around full moon. The exposure times for each filter on each night are  $8 \times 113$  s for  $g_{P1}$  and  $r_{P1}$ , and  $8 \times 240$  s for the rest. Each night the eight exposures are dithered through the Image Processing Pipeline (IPP; Magnier



**Figure 2.** Observation log of the PS1 MD04 field. Each red vertical line marks the night observed. Each row shows the survey condition in different bands. The plot shows that the survey is divided into three periods, the length of each is denoted by the blue text in the upper row.

2006; Magnier et al. 2016) and combined into nightly stacks of durations 904 and 1902 s, producing a  $5\sigma$  depth of  $r \sim 23.3$ .

Survey cadence with coupling of filters are critical for selecting OA candidates. The actual cadences of the survey with individual filters for MD04 are shown in Figure 2, where we can see that the survey is divided into three survey periods over the span of  $\sim 2$  yr (from 2011 December to 2014 January). Each survey period lasts about 3 to 4 months. There were 115 nights for the first year, 125 nights for the second year, and 80 nights for the third year, resulting in a total of 320 nights. To calculate the total effective OA survey term, we excluded the isolated nights, which are separated by more than 20 nights from other observations, since these are only snapshots and cannot be used to identify a transient. Thus, the exact number of the effective OA survey term is 154 nights. This effective survey term is used for calculation of the expected OA rate in Section 5.1.

The IPP for MDS image processing was originally located at the Maui High-Performance Computing Center, and has been moved to the Information Technology Center at University of Hawaii. It has several nightly processing stages: First, in the Chip Processing stage, the individual CCD chips are detrended and sources are detected and characterized. Then, in the Camera Calibration stage, the CCDs of each full exposure are calibrated. The images are later geometrically transformed into common pixel-grid images (called skycells) in the Warp stage. These skycell images are then combined to generate nightly images in the Stack stage. Next, source detection is performed in the Stack Photometry stage in all five filter stack images at the same time. Convolved galaxy models are fitted in the Forced Galaxy Models stage. Finally, in the Difference Image stage, nightly stacks are compared to a template reference stack for MDS fields.

#### 3.2. SUBARU/HSC Observations

Subaru is an 8.2 m telescope located at the summit of Maunakea, Hawaii. The Hyper Suprime-Cam (HSC; Miyazaki et al. 2015, 2018) is a wide-field imaging camera with an FOV of diameter 1.5 deg and  $116\,2048 \times 4096$  pixel CCDs ( $0''.168$  per pixel), mounted on the prime focus of Subaru. Under the Hyper Suprime-Cam Subaru Strategic Program (HSC-SSP; Aihara et al. 2018), three-layered (Wide, Deep, and Ultradeep), multiband ( $griz$  plus narrowband filters) imaging surveys have been executed, starting in 2014. In this paper, we use the Deep

and UltraDeep data, which have survey fields overlapping the PS1 MD04 field: E-COSMOS and COSMOS, respectively. E-COSMOS has four pointings in the Deep layer, and overlaps COSMOS, which has one pointing in the UltraDeep layer.

Only six filters can be used in a single observing run, so typically four or five broadband filters plus one or two narrowband filters are used. The exposure times are as follows: For the Deep layer, a single exposure lasts 3 minutes for the  $g$  and  $r$  bands, and 4.5 minutes for the  $i$ ,  $z$ , and  $y$  bands. For each field, 3–5 exposures are taken on each night in each filter. For the UltraDeep layer, a single exposure lasts 5 minutes for all broad bands, and 3–10 exposures are taken in one night. A more complete description of the HSC survey is provided by Aihara et al. (2018).

Images are processed through the hscPipe pipeline, which consists of four stages: The CCDs from each visit are calibrated in the CCD Processing stage. Then observations from different visits are further calibrated in the Joint Calibration stage. Subsequently, images from different visits, including observations on different nights, are combined into a deeper coadded image in the Image Coaddition stage, which is further processed in the Coadd Processing stage to detect and measure objects. The pipeline is fully described in Bosch et al. (2018). The astrometry and photometry are calibrated against the PS1 PV2 catalog. The process resulted in reduced data with an astrometric accuracy of 30 mas and a photometric accuracy of  $\sim 2\%$  (Tanaka et al. 2017). We use the s16a data release of HSC SSP, which contains the data obtained from 2016 January to April processed and merged with the s15b data release, that is, SSP data taken from 2014 March to 2015 November. The depths of images with  $5\sigma$  confidence levels for point sources are  $r$  mag  $\sim 27.1$  (Deep) and 27.7 (UltraDeep).

### 3.3. Complementary UV and NIR Data

In order to optimize the photometric redshift estimation for the hosts, complementary UV and NIR data are required. In addition to Subaru/HSC data, we used near-infrared data ( $y$ ,  $J$ ,  $H$ , and  $K_s$  band) from the UltraVista data release 3 (McCracken et al. 2012), and  $U$ -band data from MUSUBI (W.-H. Wang et al. 2020, in preparation) and CLAUDS (Sawicki et al. 2019) to generate the spectral energy distribution (SED) of hosts, and compute their photometric redshifts. The photometry used is aperture 2 magnitude. MUSUBI, which stands for Megacam UltraDeep Survey with  $U$ -Band Imaging, is a  $U$ -band complementary data set for the HSC UltraDeep layer. CLAUDS, which stands for CFHT Large-Area  $U$ -band Deep Survey, is a  $U$ -band complementary data set for the HSC Deep layer. MegaCam has two  $U$ -band filters  $u^*$  and  $u$  (Sawicki et al. 2019). In this survey, the data from both MUSUBI and CLAUDS used the  $u^*$  filter.

## 4. Results and Analysis

### 4.1. Overview of Analysis

OA searches were performed based on the flowchart shown in Figure 1. Here, we describe the four steps of our analysis: (1) identification of transients with durations shorter than 15 days from the PS1-MD04 data (Section 4.2); (2) identification of host galaxies and assessment of transient positions within them using the Subaru/HSC survey (Section 4.3) and available galaxies catalogs; (3) estimation of photometric redshift (Section 4.4); and (4) classification of transients (Section 4.5). Utilizing these

results, we examine whether the transients have the expected properties of OAs.

### 4.2. Identification of Transients

For transient identification, we used the difference catalog produced by the PS1 Transient Science Server (TSS; Gezari et al. 2012; McCrum et al. 2015). TSS creates difference images by comparing nightly stacks made by IPP compared to manually created reference images. Point-spread function fitting photometry is performed on the difference images and catalogs of transients are produced.

We imported individually detected transient candidates from each difference catalog into a custom-made PostgreSQL database and performed cross-matching with their locations. For the cross-matching, we set a search radius of  $1''$  for matching identical objects, and assigned a count number representing the number of multiple detections with different filters and/or epochs, which is useful to exclude noise events. The location of each multidetection transient was taken to be the average location of the individual detections. In total, 136,657 transient candidates were identified in the PS1-MD04 field after importing all difference catalogs made during the 2 yr of the survey.

We selected short duration candidates by applying two criteria: (selection-A) count number  $\geq 3$  and observed duration  $< 15$  days; (selection-B) count number = 2, observed duration  $< 4$  days, and a decaying light curve. The duration cut for the count = 2 case was chosen to be shorter on the grounds that, since the rising phase is more rapid than the decaying phase, if an OA can only be detected twice, its rising phase is too rapid to be detected, and only its rapid decaying phase is detectable. Transients with count = 1 are not considered for candidate selection because they are more likely to be noise. Among the 136,657 transients, 2072 of them met the criterion (selection-A) and 1402 of them met the criterion (selection-B), resulting in 3474 transients for host galaxy analysis.

### 4.3. Identification of Host Galaxies

We looked for host galaxies using Subaru/HSC data for the 3474 short duration transients selected in the previous section. The hosts were identified by cross-matching transient positions with the HSC Deep and UltraDeep catalogs in the s16a data release and selecting galaxies within a  $1''$  radius of the transient. Since the HSC astrometry were performed against with the PS1 PV2 catalog, we used the PS1 transient positions with the HSC catalogs. If multiple hosts were identified, we selected the nearest one. We also checked cutout images to exclude noise and bright stars. The transient's location within the host was computed by comparing the difference between the transient's coordinates and the host galaxy's coordinates. Multidetection transient coordinates were taken to be the average of the values from individual filters, while the host galaxy coordinates were determined in the HSC pipeline by comparing and merging peaks from different bands using the priority order irzyg (Bosch et al. 2018). Out of the 2072 transients meeting the criterion (selection-A) and the 1402 transients meeting the criterion (selection-B), 826 and 301, respectively, had identifiable hosts. These hosts were then cross-matched with the  $u^*$ -band and NIR catalogs mentioned in Section 3.3 to obtain multiband SED for photometric redshift fitting. Not all hosts have complete multiband data; the number

**Table 1**  
Photometric Redshift Results for PS1 Transients

Combination <sup>a</sup>	HSC udeep		HSC deep		All (udeep+deep)	
	Total	zphot > 2	Total	zphot > 2	Total	zphot > 2
$u^*(m)$ +optical+ir	295	55	22	4	317	59
$u^*(c)$ +optical+ir	2	0	0	0	2	0
$u^*(m)$ +optical	133	52	97	37	230	89
$u^*(c)$ +optical	12	5	430	106	442	111
optical+ir	5	1	1	0	6	1
optical	22	9	108	51	130	60
Total	469	122	658	198	1127	320 (28%) <sup>b</sup>

**Notes.**

<sup>a</sup>  $u^*(m)$  refers to MUSUBI  $u^*$ -band,  $u^*(c)$  refers to CLAUDS  $u^*$ -band, optical refers to HSC s16a data release, and ir refers to UltraVista data release 3.

<sup>b</sup> The percentage denotes the fraction of transients with zphot > 2 relative to the total number of transients.

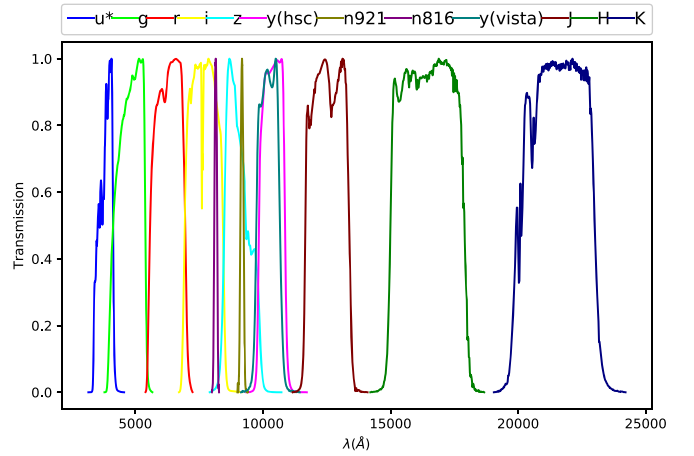
of hosts matched with various combinations of bands is summarized in Table 1. In total, we identified 1127 hosts suitable for fitting.

#### 4.4. Photometric Redshift

We used Le Phare to estimate photometric redshifts for the 1127 host galaxies. Le Phare is a Fortran program that uses the least  $\chi^2$  method to perform SED fitting with templates of stars, quasars, and galaxies (Arnouts et al. 1999; Ilbert et al. 2006). There are several libraries for galaxy fitting; instead of choosing a specific library, we merged all the templates of the default libraries into a single list so that the fitting could be performed on all the galaxy libraries. In total, there are 305 templates for galaxy fitting. We used filter responses based on each instrument’s description. For the U and optical bands, we used those given in the filt/cosmos/ directory of the Le Phare package: u\_megaprime\_sagem.res, g\_subaru.res, r\_subaru.res, i\_subaru.res, z\_subaru.res, WFCAM\_Y.res, NB921.pb, NB816.pb. Since there were no UltraVista filter response files in the package, we used the files obtained from the website of Peter L. Capak at California Institute of Technology.<sup>13</sup> The filter response files are plotted in Figure 3. The cosmological parameters used were  $H_0 = 70$ ,  $\Omega_0 = 0.3$ , and  $\Lambda_0 = 0.7$ . The redshift step used was  $dz = 0.4$ , and the maximal redshift for fitting was set at  $z_{\max} = 6$ . No extinction laws were employed in the SED fitting.

We performed a quality assessment of the photometric redshifts by comparing our photometric samples to the spectroscopic redshift catalog in the COSMOS field, PRIMUS data release 1 (Cool et al. 2013). From the catalog we selected sources with zspec quality = 3 or 4 (where zquality = 4 is the highest-quality redshift with  $\sigma_{\delta z}/(1+z) \sim 0.005$  and zquality = 3 is redshift with  $\sigma_{\delta z}/(1+z) \sim 0.022$ ).

We assess the photometric redshift quality considering six different combinations of survey catalogs for each of the two HSC catalogs (Deep and UltraDeep), which are listed in Table 1, because not all host galaxies of our selected transients have full SED data coverage. We chose 20% of redshift error (zph\_err) as the boundary of outliers, where  $zph\_err = \frac{|z_{\text{spec}} - z_{\text{phot}}|}{z_{\text{spec}} + 1}$ . Figures 4 and 5 show the quality of Le Phare on the PRIMUS catalog and the percentage of outliers. The left and right columns

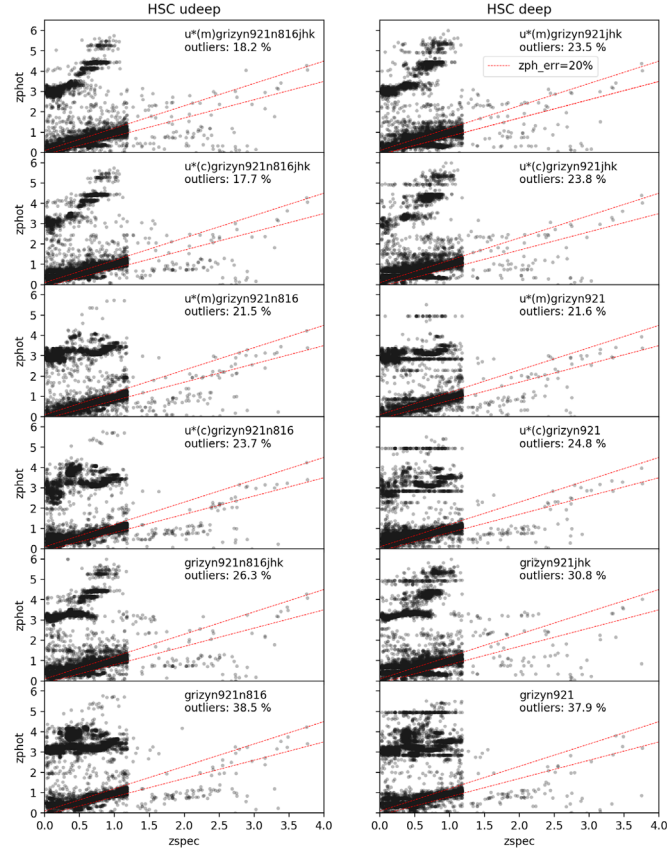


**Figure 3.** Filter response used for SED fitting. In the legend, y(hsc) refers to the HSC y band, while y(vista) refers to the UltraVista y band.

of the scatter plot in Figure 4, as well as those of the histogram in Figure 5, are zphot computed with the HSC s16a udeep and HSC s16a deep catalogs, respectively, as specified above each column. Each row corresponds to each of the six combinations of survey catalogs. The red dashed line in Figure 4 is the line where zph\_err = 20%. “Total” in Figure 5 refers to the number of multiband data computed. “Outliers” refers to the fraction of those with zph\_err > 20%. We see that by adding  $u^*$ -band data, we can reduce the fraction of outliers by 8%. The scatter plot shows that most of the data lie within the two dashed lines. This result indicates that there are significant outliers with zphot > 2 that merit additional careful examination for host object classification.

The distribution of the photometric redshifts for our 1127 hosts from PS1 transients is shown in Figure 6. The number of host galaxies with zphot > 2 from our PS1 transients for various combinations of multiband SED is shown in Table 1. The photometric redshifts indicate that about 30% of our host galaxy samples fall into the range of zphot > 2. These outlier samples had better SED fits with star or QSO models than with galaxy templates. We also examined cutout images and found that most of these objects showed point-like features. The relatively small position differences between the transients and these point-like hosts also strongly suggested that these outlier samples might be stars. Hence, we classified all the outliers as stars or QSOs.

<sup>13</sup> <http://www.astro.caltech.edu/~capak/filters/index.html>



**Figure 4.** Scatter plot of  $z_{\text{phot}}$  quality using the  $z_{\text{spec}}$  catalog. Dashed lines are  $z_{\text{ph\_err}} = 20\%$ . Outliers refer to the fraction of  $z_{\text{ph\_err}} > 20\%$ .  $z_{\text{phot}}$ —left column: HSC udeep ( $g, r, i, z, y, \text{nb921}$ , and  $\text{nb816}$  bands), UltraVista ( $y, j, h$ , and  $ks$  bands), MUSUBI ( $u^*$ -band), CLAUDS ( $u^*$ -band); right column: HSC deep ( $g, r, i, z, y$ , and  $\text{nb921}$  bands), UltraVista ( $y, j, h$ , and  $ks$  bands), MUSUBI ( $u^*$ -band), and CLAUDS ( $u^*$ -band).  $z_{\text{spec}}$ : G10CosmosCat PRIMUS.  $u^*(c)$  refers to CLAUDS ( $u^*$ -band), while  $u^*(m)$  refers to MUSUBI ( $u^*$ -band).

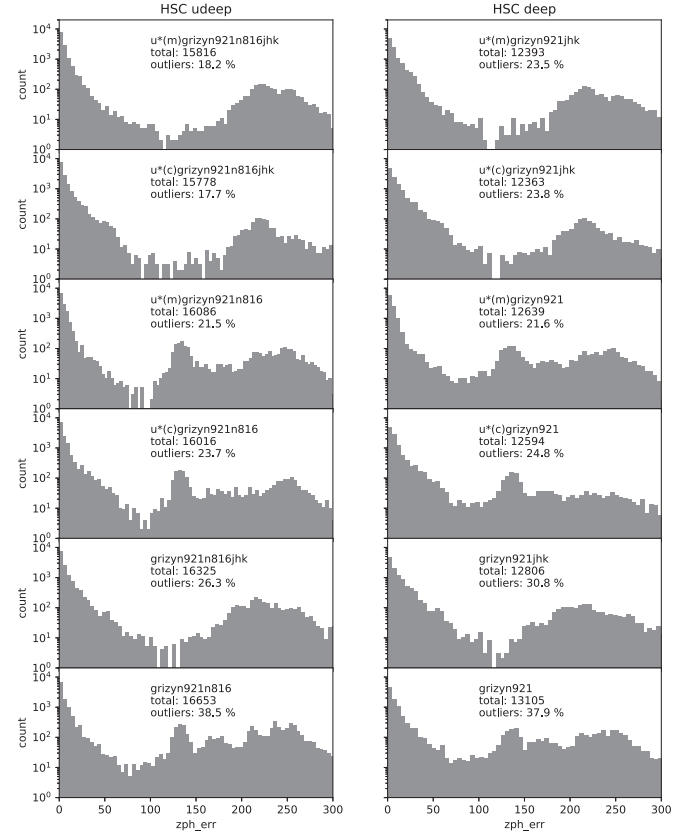
We converted apparent magnitudes of transients to absolute magnitude ( $M_{\text{abs}}$ ) based on  $z_{\text{phot}}$ . The  $M_{\text{abs}}$  is calculated by using the distance module calculator<sup>14</sup> (Wright 2006).

#### 4.5. Known Source Identification

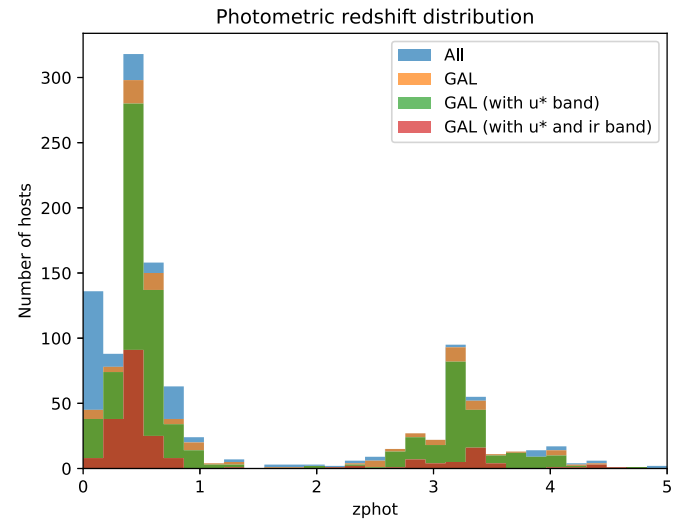
After an initial examination by eye, we excluded events with bright hosts and flat or variable (decaying, then rising) light curves. We selected  $\sim 150$  events with faint hosts or OA-like light-curve variations, and performed cross-matching against various catalogs using Simbad and VizieR. By cross-matching, we can exclude the known transients and focus on unidentified ones. We found that most of the transients, whether or not they were  $z_{\text{phot}}$  outliers, had star-like or bright hosts. (GRB hosts, by contrast, tend to be faint and small and are of course not star-like). Out of the  $\sim 150$  events,  $\sim 20$  events had hosts detectable in X-ray or radio band, which we excluded as probable AGNs.

#### 4.6. Selection of Orphan GRB Afterglows

For each of the 1127 transients with hosts identified, we generated an individual event summary including the cutout images of host galaxies,  $z_{\text{phot}}$  result of host galaxies, and light curve of transients with a scale of their absolute magnitude; we

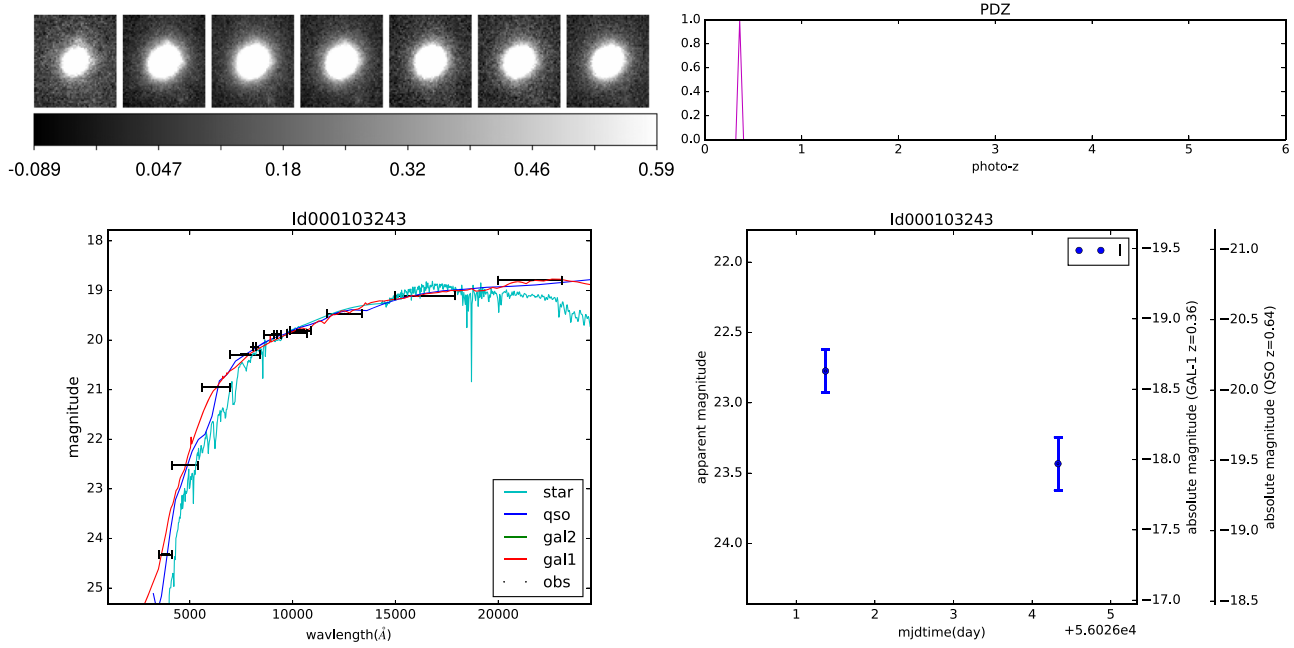


**Figure 5.** Histogram of  $z_{\text{phot}}$  quality using the  $z_{\text{spec}}$  catalog. Total number of  $z_{\text{spec}}$  data used is specified. Outliers refer to the fraction of  $z_{\text{ph\_err}} > 20\%$ .  $z_{\text{phot}}$ —left column: HSC udeep ( $g, r, i, z, y, \text{nb921}$ , and  $\text{nb816}$  bands), UltraVista ( $y, j, h$ , and  $ks$  bands), MUSUBI ( $u^*$ -band), CLAUDS ( $u^*$ -band); right column: HSC deep ( $g, r, i, z, y$ , and  $\text{nb921}$  bands), UltraVista ( $y, j, h$ , and  $ks$  bands), MUSUBI ( $u^*$ -band), and CLAUDS ( $u^*$ -band).  $z_{\text{spec}}$ : G10CosmosCat PRIMUS.  $u^*(c)$  refers to CLAUDS ( $u^*$ -band), while  $u^*(m)$  refers to MUSUBI ( $u^*$ -band).



**Figure 6.** Photometric redshift distribution of 1127 hosts from PS1 transients. Blue refers to the photometric redshift result for all 1127 hosts, which include hosts classified as galaxies, QSO, or stars in Le Phare. Orange refers to the subset of hosts that are classified as galaxies in Le Phare. Green refers to the subset of hosts that are classified as galaxies and have  $u^*$ -band data in their SED. Red refers to the subset of hosts that are classified as galaxies and have  $u^*$ -band and  $ir$  data in their SED.

<sup>14</sup> <http://www.astro.ucla.edu/~wright/CosmoCalc.html>



**Figure 7.** Example transient. Top left: Multiband cutout images of the host galaxy from HSC s16a. From left to right they are  $g$ ,  $r$ ,  $i$ ,  $z$ ,  $y$ ,  $nb816$  and  $nb921$  bands. The transient is located at the center of each cutout image. Bottom left: SED fitting result of the host galaxy from Le Phare. Gal1 refers to the best-fitted galaxy template, while gal2, if there is one, refers to the second best. Top right: photo- $z$  probability distribution. Note that this is for galaxy templates only. Bottom right: light curve with apparent magnitude on the left scale and absolute magnitude on the right. The absolute magnitudes are calculated using the redshift obtained from Le Phare, which is specified in the parenthesis of the y label on the right. We discuss and conclude that this transient is not an OA but possibly an AGN in Section 4.6.

classified the transients by examining this combined information. We show an example in Figure 7 to demonstrate our selection process. This transient has an observed duration of  $\sim 3$  days and a decaying light curve. Multiband data from  $u^*$ -band, optical, and IR give us a  $z_{\text{phot}}$  of 0.36. The cutout images show that the host is very bright, and thus unlikely to be an OA host. From cross-matching catalogs, we find in Simbad that it is a galaxy in the Advanced Camera for Surveys-General Catalog with  $z_{\text{spec}} = 0.3396$ , which is highly consistent with our  $z_{\text{phot}}$  result. It also has detections in the Chandra and XMM-Newton surveys. As a result, we conclude that it is unlikely to be an OA, but could be an AGN.

After careful examinations, we concluded that no OA candidates were found. Most of the transients had too few light-curve points to show any significant properties, and none of them met the duration selection criteria. The light curves of those with more data points were usually either very flat, or had variation amplitudes that were too small ( $< 1$  magnitude) when compared to the theoretical OA light curves. From the cutout images and SED, most host galaxies appeared to be very bright and large, while the expected host properties of OAs are dwarf galaxies, with relatively fainter magnitudes and redshifts around 1–2. We were not able to find a candidate with both an interesting light curve and host properties strongly indicative of being an OA. We summarize our selection process and result in Table 2.

## 5. Discussion

### 5.1. Comparison with Theoretical Expectations

The theoretically predicted rate of OAs depends on the model used. Here we compute and compare with our null result the expected rate in the PS1 MD04 field using models from three different theoretical papers: T02, R08, and N02. We assume a survey area  $\Omega_{\text{obs}}$  of  $7 \text{ deg}^2$ , and a limiting magnitude

Table 2 Summary of Number of Candidates Remaining after Each Selection Cut		
Selection Criteria	Number	
Database of differential images from PS1 MD04	136,657	
Duration $t$ , count, and light curve	$\geq 3$ detections within 15 days	$= 2$ detections within 4 days & decaying
	2072	1402
Host in HSC	826	301
Examine host galaxies, light-curve properties, $z_{\text{phot}}$ , and cross-matching catalogs	0	

in  $R$  band  $\sim 23$ . We use 154 nights with 1–13 nights' separation and a total observing time of 320 nights to compute the number of expected OAs, following the respective calculation methods in each of the three papers. In the following calculations,  $N_{\text{oa}}$  is the number of OAs expected to be observed in our survey;  $N_{\text{snap}}$  is the number of OAs in one snapshot of the whole sky;  $T_{\text{obs}}$  is the total observing time (320 nights);  $T_{\text{oa}}$  is the lifetime of an OA. To identify a transient, we need to consider the consecutive monitoring condition, which we define as the density of the log file shown in Figure 2. In our rate calculations we define a survey efficiency  $\text{eff}$  equal to this density, which is  $154/320 \sim 0.5$ .

T02 used GRB parameters from an average of 10 well-studied events. From this model and Table 1 of T02, we found that  $N_{\text{snap}} = 330$  can reproduce the expected 36 OAs with a sensitivity of  $R \sim 23$  and effective survey area of about  $4500 \text{ deg}^2$ . We use  $N_{\text{snap}} = 330$  and the  $\langle 1/T_{\text{oa}} \rangle^{-1} \sim 18$  days from Table 1 of T02 for SDSS to estimate detection rate with our

cadence.

$$N_{\text{oa}} = N_{\text{snap}} \cdot \frac{\text{equivalent snapshot area}}{4\pi} \quad (1)$$

$$= N_{\text{snap}} \cdot \frac{T_{\text{obs}}}{\langle 1/T_{\text{oa}} \rangle^{-1}} \cdot \frac{\Omega_{\text{obs}}}{4\pi} \cdot \text{eff} \quad (2)$$

$$= 330 \cdot \frac{320 \text{ day}}{18 \text{ day}} \cdot \frac{7 \text{ deg}^2}{4\pi} \cdot \left( \frac{\pi}{180 \text{ deg}} \right)^2 \cdot 0.5 \quad (3)$$

$$\simeq 0.5, \quad (4)$$

which is smaller than one but not exactly zero. However, the OAs considered by T02 are bright, yielding average lifetimes that are too long ( $\langle 1/T \rangle^{-1} \sim 18$ ). If we instead considered an average lifetime of about a week at this sensitivity (e.g., Kann et al. 2010), we would obtain an expected number of 1 to 2 OAs, which is larger than our null result.

R08 considered the USJ model, which has a wide outflow  $\theta_{\text{jet}} = 90^\circ$  and an angle-dependent energy distribution  $E(\theta) \propto \theta^{-2}$ . They suggested that if the consecutive monitoring  $T_{\text{obs}}$  is longer than the OA mean lifetime  $T_{\text{th}}$ , then the number of OAs is

$$N_{\text{oa}} = R_{\text{oa}} \cdot T_{\text{obs}} \cdot \frac{\Omega_{\text{obs}}}{4\pi}, \quad (5)$$

where  $R_{\text{oa}}$  is the mean rate that OAs appear in the sky over the survey flux threshold. At  $R \sim 23$ , according to the calculations for the expected rate of the survey conducted by Rau et al. (2006) in R08,  $T_{\text{th}} \sim 22$  and  $R_{\text{oa}} \sim 6.3 \text{ day}^{-1}$ . Putting these parameters as well as the survey efficiency  $\text{eff}$  into Equation (6) we obtain

$$N_{\text{oa}} = 6.3 \text{ day}^{-1} \cdot 320 \text{ day} \cdot \frac{7 \text{ deg}^2}{4\pi} \cdot \left( \frac{\pi}{180 \text{ deg}} \right)^2 \cdot 0.5 \simeq 0.2. \quad (6)$$

N02 considered a jet with constant maximal OA observing angle  $\theta_{\text{max}}$  that is independent of  $\theta_{\text{jet}}$  (for  $\theta_{\text{jet}} < \theta_{\text{max}}$ ), with two jet opening angles. The “canonical” model (N02C) used  $\theta_{\text{jet}} = 0.1$  radian, which is similar to the averaged jet opening angle. The “optimistic” model (N02O) used  $\theta_{\text{jet}} = 0.05$  radian, which is even smaller than observed typical jet opening angle (e.g., Racusin et al. 2009). They did not give a characteristic lifetime of OAs, but stated that for most OAs, if the separation between observed nights is longer than 2 weeks, then the two observations can be considered independent. We obtain  $N_{\text{snap}}$  values from Figure 3 of N02, which is also supported by Figure 8 of R08. Using  $T_{\text{oa}} \sim 14$ ,  $N_{\text{snap}} \sim 70$  (N02O), and  $N_{\text{snap}} \sim 1.7$  (N02C), we find the estimated number of OAs to be:

$$N_{\text{oa}} = N_{\text{snap}} \cdot \frac{T_{\text{obs}}}{T_{\text{oa}}} \cdot \frac{\Omega_{\text{obs}}}{4\pi} \cdot \text{eff} \quad (7)$$

$$= 70 \cdot \frac{320 \text{ day}}{14 \text{ day}} \cdot \frac{7 \text{ deg}^2}{4\pi} \cdot \left( \frac{\pi}{180 \text{ deg}} \right)^2 \cdot 0.5 \quad (8)$$

$$\simeq 0.1 \text{ (N02O)} \quad (9)$$

$$N_{\text{oa}} = 1.7 \cdot \frac{320 \text{ day}}{14 \text{ day}} \cdot \frac{7 \text{ deg}^2}{4\pi} \cdot \left( \frac{\pi}{180 \text{ deg}} \right)^2 \cdot 0.5 \quad (10)$$

$$\simeq 0.003 \text{ (N02C)}. \quad (11)$$

**Table 3**

Predicted Number of OAs in PS1 MD04 Using Different Models

Model	$10^{(\log_{10} T)}$ (day) <sup>a</sup>	$\langle 1/T \rangle^{-1}$ (day)	$N_{\text{snap}}$ (all sky)	$N_{\text{oa}}$	$N_{\text{oa}}$ (one week lifetime) <sup>b</sup>
T02	32	18	330	0.5	1.3
R08	22	2	12	0.2	0.05
N02O	...	...	70	0.1	0.3
N02C	...	...	1.7	0.003	0.006

**Notes.** N02 did not give the lifetimes  $10^{(\log_{10} T)}$  and  $\langle 1/T \rangle^{-1}$ , so they are left blank. But they mentioned that two weeks can be considered as an average lifetime of OAs. Therefore, we used  $T \sim 14$  for their  $N_{\text{oa}}$  calculation.

<sup>a</sup>  $T_{\text{th}}$  in R08.

<sup>b</sup> Calculated with a shorter lifetime (one week) than the lifetime originally considered in the models.

Table 3 shows  $N_{\text{oa}}$  calculated by the above models with the given parameters.

In summary, R08 predicts 0.2 OAs, which we find consistent with our result. Even though R08 considered a very short lifetime  $\langle 1/T \rangle^{-1} \sim 2$ , the predicted number of OAs would be still closer to zero ( $N_{\text{oa}} \sim 0.05$ ) if we increase the lifetime to a week. Thus, we find R08 consistent with our result in this case also. N02O predicts 0.1 OAs considering an average lifetime of two weeks. Reducing the lifetime to one week would increase the  $N_{\text{oa}}$  to 0.2, which we find consistent with our result. N02C, the most pessimistic of the models we considered, predicts 0.003 OAs; this, too, is consistent with our null result.

## 5.2. Toward Further Surveys

We next discuss methods to evaluate the rate predictions of the models R08 and N02. If we were to examine all 10 fields of the PS1 Medium Deep Survey, R08 and N02O predict that we would find one or two OAs, each of which could be further evaluated. But N02C predicts 0.03 OAs, indicating that we would be still unlikely to find an OA in this survey. With the same survey area ( $7 \text{ deg}^2 \times 10$ ), number of observing nights, and survey efficiency, N02C requires a limiting magnitude of  $R \sim 25$  to detect 1 OA. Therefore, we will need a more efficient survey to evaluate N02C.

From the above calculations, we can see that  $N_{\text{snap}}$  varies greatly from model to model. However,  $\langle 1/T_{\text{oa}} \rangle^{-1}$  also varies by roughly the same order, leading to same-order values of  $N_{\text{oa}}$ . To distinguish between the various models, we find continuous monitoring for a week each month for a year is preferred over observing 84 nights continuously, since at a sensitivity of  $R \sim 23$  we can regard the monthly survey as 12 snapshots and would not have to consider the various characteristic lifetimes. Depending on the model, the monthly survey might produce a higher  $N_{\text{oa}}$  than the continuous 84 nights survey, but it might also increase the difficulty of classifying transients.

As of its second data release (dr2), HSC has observed 174 nights (Aihara et al. 2019). The Deep survey monitored four fields, amounting to a total area of  $\sim 26 \text{ deg}^2$ . The cadence for each field each year obtained from dr2 is roughly two weeks per month over the course of two to four consecutive months. The Ultra Deep survey observed two fields, with a total area of  $\sim 4 \text{ deg}^2$ . The cadence for each field is roughly one to two weeks every one or two months over the course of half a year. Using the aforementioned cadence of HSC dr2 and the four models described in Section 5.1, the predicted number of OAs and the parameters used for the calculations are summarized in

**Table 4**  
Predicted Number of OAs for HSC, LSST, and WFIRST Using Different Models

Survey	Mag	Area (deg <sup>2</sup> )	$\langle T_{\text{obs}} \rangle$			$10^{(\log_{10} T)}$ (day) <sup>b</sup>	$\langle 1/T \rangle^{-1}$		$N_{\text{snap}}$				$N_{\text{oa}}$			
			(day yr <sup>-1</sup> ) <sup>a</sup>				(day) <sup>c</sup>		(all sky)				(yr <sup>-1</sup> )			
			T02	R08	N02		R08	T02	R08	T02	R08	N02O	N02C	T02	R08	N02O
HSC Deep	R: 26	26	96	103	22	170	97	22	5000	200	1000	40	4	0.2	2	0.07
HSC UltraDeep	R: 27	4	101	263	25	300	180	70	15000	450	2000	80	1	0.1	0.5	0.02
LSST	R: 24.5	3300	365	365	365	60	40	8	1200	55	250	8	885	203	527	17
WFIRST Wide	J: 27.5	27.44	91	91	91	500	300	150	50000	1200	6000	300	17	0.4	26	1.3
WFIRST Medium	J: 27.6	8.96	91	91	91	500	300	150	50000	1200	6000	300	5	0.1	9	0.4
WFIRST Deep	J: 29.3	5.04	91	91	91	1200	700	600	170000	4000	30000	2000	10	0.2	24	1.6

**Notes.** For estimations of HSC surveys, we use the cadence obtained from the HSC second data release (Aihara et al. 2019). LSST will cover 10,000 deg<sup>2</sup> every three days. The three layers of WFIRST SN Survey (wide, medium, and deep) will have a survey duration of 0.5 years over a 2 yr interval, and a cadence of 5 days (Spergel et al. 2013).

<sup>a</sup> For HSC surveys this is the yearly effective survey duration averaged over the multiple fields, which is a rough estimate of the actual effective survey duration used for the calculations.

<sup>b</sup>  $T_{\text{th}}$  in R08.

<sup>c</sup> For N02 models we used  $T \sim 14$ , same as that in Table 3.

Table 4. Note that  $\langle T_{\text{obs}} \rangle$  for HSC in Table 4 shows the yearly effective survey duration averaged over the multiple fields, which is only a rough estimate of the actual effective survey duration used for the calculations. The HSC survey would be able to verify the N02O case as summarized in Table 4. LSST will image 10,000 deg<sup>2</sup> every three nights, with a limiting magnitude of  $R \sim 24.5$  (Ivezić et al. 2019; LSST Science Collaboration et al. 2017). We used these survey parameters of LSST to obtain the expected numbers of OAs in Table 4. LSST would be able to verify all four model cases in Table 4. Our expected numbers of OAs for T02 and N02C are in the same order as estimations by LSST Science Collaboration et al. (2009; i.e.,  $N_{\text{oa}} \sim 1000$ , which used the T02 model) and by Ghirlanda et al. (2015; i.e.,  $N_{\text{oa}} \sim 50$ , which used a population synthesis code), respectively. We also calculated the expected numbers of OAs with the planned SN survey using the WFIRST mission (Spergel et al. 2013). In Table 4, we summarized the results for three layers of SN surveys (wide, medium, and deep) with the limiting magnitude of  $J$ -band, the cadence of 5 days, and the planned survey duration of 0.5 years in a 2 yr interval. Since the satellite based time-domain survey would maintain the planned cadence (i.e., unaffected by weather condition unlike ground-based observations), the WFIRST survey would also be essential for the OA surveys. Subaru/HSC, LSST, and WFIRST therefore are promising surveys for discovering OAs.

## 6. Conclusion

In an attempt to find OAs, we used the MD04 field of the Pan-STARRS1 Medium Deep Survey, which covers an area of 7 deg<sup>2</sup> overlapping with the COSMOS field, has a limiting magnitude reaching  $R \sim 23$ , and observed 154 nights over the course of 2 years (from 2011 December to 2014 January). We identified 136,657 transients by generating differential images, and then performed transient classification. We reduced the number to 1127 by excluding long duration and hostless transients, and then checked carefully each remaining candidate’s host galaxy, location in the host, light-curve properties, and  $z_{\text{phot}}$ , cross-matching the results with other catalogs. For  $z_{\text{phot}}$ , we used MUSUBI, CLAUDS, HSC, and UltraVista to construct the SED of each transient, and then performed SED

fitting using Le Phare. We checked our  $z_{\text{phot}}$  quality using a  $z_{\text{spec}}$  catalog PRIMUS and found that we could reduce the fraction of outliers ( $z_{\text{ph\_err}} > 20\%$ ) down to 18%, which we consider acceptable. After careful examination we concluded that we did not find any OA candidates.

We then compared our result with the expected number of OAs computed using different models: T02, R08, N02O, and N02C which predicts 0.5, 0.2, 0.1, and 0.003 OAs, respectively. R08 and N02 are consistent with our result. We find the average lifetime of OAs in T02 is too long ( $\langle 1/T_{\text{oa}} \rangle^{-1} \sim 18$ ); reducing it would increase  $N_{\text{oa}}$  to  $1 \sim 2$ , which we consider to be marginally consistent with our result. We may be able to evaluate R08 and N02O by examining all 10 fields of PS1 Medium Deep Survey, but the evaluation of N02C would require a more efficient survey.

HSC is 3–4 magnitudes deeper than PS1, which should result in a higher rate of OA candidate detections, and probably in a discovery. However, LSST is the most promising survey to detect OAs, and will detect a larger number than other optical surveys.

The Pan-STARRS1 Surveys have been made possible through contributions of the Institute for Astronomy, the University of Hawaii, the Pan-STARRS Project Office, the Max-Planck Society and its participating institutes, the Max Planck Institute for Astronomy, Heidelberg and the Max Planck Institute for Extraterrestrial Physics, Garching, The Johns Hopkins University, Durham University, the University of Edinburgh, Queens University Belfast, the Harvard-Smithsonian Center for Astrophysics, the Las Cumbres Observatory Global Telescope Network Incorporated, the National Central University of Taiwan, the Space Telescope Science Institute, the National Aeronautics and Space Administration under grant No. NNX08AR22G issued through the Planetary Science Division of the NASA Science Mission Directorate, the National Science Foundation under grant No. AST-1238877, the University of Maryland, Eotvos Lorand University (ELTE), and the Los Alamos National Laboratory.





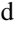

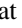
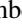
The Hyper Suprime-Cam (HSC) collaboration includes the astronomical communities of Japan and Taiwan, and Princeton University. The HSC instrumentation and software were

developed by the National Astronomical Observatory of Japan (NAOJ), the Kavli Institute for the Physics and Mathematics of the Universe (Kavli IPMU), the University of Tokyo, the High Energy Accelerator Research Organization (KEK), the Academia Sinica Institute for Astronomy and Astrophysics in Taiwan (ASIAA), and Princeton University. Funding was contributed by the FIRST program from Japanese Cabinet Office, the Ministry of Education, Culture, Sports, Science and Technology (MEXT), the Japan Society for the Promotion of Science (JSPS), Japan Science and Technology Agency (JST), the Toray Science Foundation, NAOJ, Kavli IPMU, KEK, ASIAA, and Princeton University. Based the HSC-SSP on data collected at the Subaru Telescope and retrieved from the HSC data archive system, which is operated by the Subaru Telescope and Astronomy Data Center at National Astronomical Observatory of Japan.

This paper makes use of software developed for the Large Synoptic Survey Telescope. We thank the LSST Project for making their code available as free software at <https://www.lsst.org/about/dm>.

This work is supported by the Ministry of Science and Technology of Taiwan grants MOST 105-2112-M-008-013-MY3 (Y.U.) and MOST 108-2112-M-001-051 (K.A.).

### ORCID iDs

Yun-Jing Huang  <https://orcid.org/0000-0002-2952-8429>  
 Yuji Urata  <https://orcid.org/0000-0001-7082-6009>  
 Yuji Shirasaki  <https://orcid.org/0000-0002-2884-2934>  
 Wei-Hao Wang  <https://orcid.org/0000-0003-2588-1265>  
 Sebastien Foucaud  <https://orcid.org/0000-0001-5603-6262>  
 Mark E. Huber  <https://orcid.org/0000-0003-1059-9603>  
 Richard Wainscoat  <https://orcid.org/0000-0002-1341-0952>  
 Kenneth C. Chambers  <https://orcid.org/0000-0001-6965-7789>

### References

- Aihara, H., AlSayyad, Y., Ando, M., et al. 2019, *PASJ*, **71**, 114  
 Aihara, H., Arimoto, N., Armstrong, R., et al. 2018, *PASJ*, **70**, S4  
 Alexander, K. D., Berger, E., Fong, W., et al. 2017, *ApJL*, **848**, L21  
 Antonucci, R. 1993, *ARA&A*, **31**, 473  
 Arnouts, S., Cristiani, S., Moscardini, L., et al. 1999, *MNRAS*, **310**, 540  
 Barthelmy, S. D., Barbier, L. M., Cummings, J. R., et al. 2005, *SSRv*, **120**, 143  
 Becker, A. C., Wittman, D. M., Boeshaar, P. C., et al. 2004, *ApJ*, **611**, 418  
 Berger, E. 2010, *ApJ*, **722**, 1946  
 Bosch, J., Armstrong, R., Bickerton, S., et al. 2018, *PASJ*, **70**, S5  
 Cenko, S. B., Urban, A. L., Perley, D. A., et al. 2015, *ApJL*, **803**, L24  
 Chambers, K. C., Magnier, E. A., Metcalfe, N., et al. 2016, arXiv:1612.05560  
 Chen, W. J., Urata, Y., Huang, K., et al. 2020, *ApJL*, **891**, L15  
 Cool, R. J., Moustakas, J., Blanton, M. R., et al. 2013, *ApJ*, **767**, 118  
 Frail, D. A., Kulkarni, S. R., Sari, R., et al. 2001, *ApJL*, **562**, L55  
 Gal-Yam, A., Ofek, E. O., Poznanski, D., et al. 2006, *ApJ*, **639**, 331  
 Gezari, S., Chornock, R., Rest, A., et al. 2012, *Natur*, **485**, 217  
 Ghirlanda, G., Salvaterra, R., Campana, S., et al. 2015, *A&A*, **578**, A71  
 Granot, J., Panaitescu, A., Kumar, P., et al. 2002, *ApJL*, **570**, L61  
 Granot, J., Ramirez-Ruiz, E., & Perna, R. 2005, *ApJ*, **630**, 1003  
 Greiner, J., Hartmann, D. H., Voges, W., et al. 2000, *A&A*, **353**, 998  
 Grindlay, J. E. 1999, *ApJ*, **510**, 710  
 Haggard, D., Nynka, M., Ruan, J. J., et al. 2017, *ApJL*, **848**, L25  
 Harrison, F. A., Bloom, J. S., Frail, D. A., et al. 1999, *ApJL*, **523**, L121  
 Ilbert, O., Arnouts, S., McCracken, H. J., et al. 2006, *A&A*, **457**, 841  
 Ioka, K., & Nakamura, T. 2018, *PTEP*, **2018**, 043E02  
 Ivezić, Ž., Kahn, S. M., Tyson, J. A., et al. 2019, *ApJ*, **873**, 111  
 Izzo, L., de Ugarte Postigo, A., Maeda, K., et al. 2019, *Natur*, **565**, 324  
 Jin, Z.-P., Li, X., Wang, H., et al. 2018, *ApJ*, **857**, 128  
 Kann, D. A., Klose, S., Zhang, B., et al. 2010, *ApJ*, **720**, 1513  
 Kathirgamaraju, A., Barniol Duran, R., & Giannios, D. 2018, *MNRAS*, **473**, L121  
 Lamb, G. P., & Kobayashi, S. 2017, *MNRAS*, **472**, 4953  
 Lamb, G. P., & Kobayashi, S. 2018, *MNRAS*, **478**, 733  
 Lamb, G. P., & Kobayashi, S. 2019, *MNRAS*, **489**, 1820  
 Lamb, G. P., Lyman, J. D., & Levan, A. J. 2019, *ApJL*, **870**, L15  
 Lamb, G. P., Tanaka, M., & Kobayashi, S. 2018, *MNRAS*, **476**, 4435  
 Law, C. J., Gaensler, B. M., Metzger, B. D., et al. 2018, *ApJL*, **866**, L22  
 Lazzati, D., López-Cámara, D., Cantiello, M., et al. 2017, *ApJL*, **848**, L6  
 Levinson, A., Ofek, E. O., Waxman, E., et al. 2002, *ApJ*, **576**, 923  
 Li, L., Wang, Y., Shao, L., et al. 2018, *ApJS*, **234**, 26  
 LSST Science Collaboration, Abell, P. A., Allison, J., et al. 2009, arXiv:0912.0201  
 LSST Science Collaboration, Marshall, P., Anguita, T., et al. 2017, arXiv:1708.04058  
 Lyman, J. D., Lamb, G. P., & Levan, A. J. 2018, *NatAs*, **2**, 751  
 Magnier, E. 2006, in The Advanced Maui Optical and Space Surveillance Technologies Conference, **E50**  
 Magnier, E. A., Chambers, K. C., Flewelling, H. A., et al. 2016, arXiv:1612.05240  
 Malacrino, F., Atteia, J.-L., Boër, M., et al. 2007, *A&A*, **464**, L29  
 Marcote, B., Nimmo, K., Salafia, O. S., et al. 2019, *ApJL*, **876**, L14  
 McCracken, H. J., Milvang-Jensen, B., Dunlop, J., et al. 2012, *A&A*, **544**, A156  
 McCrum, M., Smartt, S. J., Rest, A., et al. 2015, *MNRAS*, **448**, 1206  
 Miyazaki, S., Oguri, M., Hamana, T., et al. 2015, *ApJ*, **807**, 22  
 Miyazaki, S., Oguri, M., Hamana, T., et al. 2018, *PASJ*, **70**, S27  
 Murguía-Berthier, A., Ramirez-Ruiz, E., Kilpatrick, C. D., et al. 2017, *ApJL*, **848**, L34  
 Nakar, E., Piran, T., & Granot, J. 2002, *ApJ*, **579**, 699  
 Piran, T. 1999, *PhR*, **314**, 575  
 Racusin, J. L., Liang, E. W., Burrows, D. N., et al. 2009, *ApJ*, **698**, 43  
 Rau, A., Greiner, J., & Schwarz, R. 2006, *A&A*, **449**, 79  
 Rhoads, J. E. 1999, *ApJ*, **525**, 737  
 Rossi, E. M., Perna, R., & Daigne, F. 2008, *MNRAS*, **390**, 675  
 Rykoff, E. S., Aharonian, F., Akerlof, C. W., et al. 2005, *ApJ*, **631**, 1032  
 Sari, R., Piran, T., & Halpern, J. P. 1999, *ApJL*, **519**, L17  
 Sawicki, M., Arnouts, S., Huang, J., et al. 2019, *MNRAS*, **489**, 5202  
 Shirasaki, Y., Kawai, N., Yoshida, A., et al. 2003, *PASJ*, **55**, 1033  
 Šimon, V., Hudec, R., Pizzichini, G., et al. 2001, *A&A*, **377**, 450  
 Spergel, D., Gehrels, N., Breckinridge, J., et al. 2013, arXiv:1305.5425  
 Tanaka, M., Hasinger, G., Silverman, J. D., et al. 2017, arXiv:1706.00566  
 Tanaka, M., Morokuma, T., Itoh, R., et al. 2014, *ApJL*, **793**, L26  
 Tonry, J. L., Stubbs, C. W., Lykke, K. R., et al. 2012, *ApJ*, **750**, 99  
 Totani, T., & Panaitescu, A. 2002, *ApJ*, **576**, 120  
 Troja, E., Piro, L., Ryan, G., et al. 2018, *MNRAS*, **478**, L18  
 Troja, E., van Eerten, H., Ryan, G., et al. 2019, *MNRAS*, **489**, 1919  
 Urata, Y., Huang, K., Yamazaki, R., et al. 2015, *ApJ*, **806**, 222  
 Urata, Y., Tsai, P. P., Huang, K., et al. 2012, *ApJL*, **760**, L11  
 Wright, E. L. 2006, *PASP*, **118**, 1711  
 Yamazaki, R., Ioka, K., & Nakamura, T. 2002, *ApJL*, **571**, L31